DMD Fast Forward. Published on June 19, 2008 as doi:10.1124/dmd.107.020271

DMD #20271

BIODISTRIBUTION OF RADIOLABELED ETHANOL IN RODENTS

Andrew N. Gifford, Mel Pilar Espaillat and S. John Gatley

Medical Department, Brookhaven National Laboratory, Upton, NY 11973

AG, MPE, SJG*

Running title: Ethanol biodistribution in rodents

Correspondence: Dr. A.N. Gifford, Medical Department, Brookhaven National Laboratory, Upton NY 11973.

Tel: 631-344-7069; Fax: 631-344-5311; email: gifforda@bnl.gov

Text pages 24

Tables 3

Figures 4

References 31

Abstract words 238,

Introduction words 354

Discussion words 1488

Abbreviations: ROI, Region of interest; %ID/g, Percent injected dose per gram

Abstract

The biodistribution of [1-^{14}C]ethanol in rodents was examined to determine sites of concentration of ethanol or its metabolites that may contribute to its toxicological and pharmacokinetic characteristics. Following intravenous administration of [1-^{14}C]ethanol in mice, radioactivity showed a widespread distribution amongst body organs. Determination of the proportion of tissue radioactivity accounted for by volatile [1-^{14}C]ethanol versus non-volatile ^{14}C metabolites indicated that tissue radioactivity was mostly in the form of the latter, even as early as 5 min post-injection, indicating a rapid metabolism of the radiolabeled ethanol to labeled metabolites. In a separate study, radioactivity was imaged using whole-body autoradiography following intravenous administration in rats. High levels of radioactivity were observed in the Harderian gland, preputial gland and in the pancreas at 15 and 60 min post-injection. High levels of radioactivity were also apparent at the later time point in the intestinal tract, indicating hepatobillary excretion of radiolabeled metabolites. Moderate levels of radioactivity were present in the liver, lungs, salivary glands, bone marrow and kidney cortex. In conclusion, following intravenous [^{14}C]ethanol administration, radioactivity initially distributes widely amongst body organs but concentrates in specific tissues at subsequent time points. Especially notable in the current study was the high concentration of radioactivity accumulating in the pancreas. It is thus tempting to speculate that the well-documented high incidence of pancreatic disease in observed in human chronic alcoholism may be related to a propensity of this organ to accumulate ethanol and/or reactive ethanol metabolites.

Determining the biodistribution of drugs in the body following oral or systemic administration is of value both for guiding toxicological studies and for identifying sites of retention of the drugs that can account for pharmacokinetic behavior. Drug levels in tissues for biodistribution studies can be quantified either using mass spectrometry for drugs that incorporate only stable isotopes, or by using autoradiography and/or scintillation counting for radiolabeled drugs.

In the case of ethanol, pharmacokinetic measurements on plasma ethanol levels in human studies indicate that ethanol has a volume of distribution approximating that of total body water (0.5 – 0.7 L/kg) and that it rapidly distributes to tissues. In animal studies, biodistribution determinations have mostly concentrated on determining the pharmacokinetics of brain uptake of ethanol (Sunahara et al., 1978; Richardson et al., 1987; Smolen and Smolen, 1989; Robinson et al., 2000; Gulyas et al., 2002; Jamal et al., 2003; Quertemont et al., 2003; Peris et al., 2006). These studies have employed both radiolabeled and unlabeled forms of ethanol and have indicated that ethanol rapidly enters the brain following systemic administration and brain levels equilibrate with blood levels.

Compared with brain studies, relatively few studies have been conducted on the whole-body organ distribution of ethanol or its metabolites. We are aware of only two animal studies that have measured the biodistribution of radiolabeled ethanol across multiple body organs (Ho et al., 1972; Akesson, 1974). Both of these studies used a film autoradiographic approach and a non-quantitative analysis of radioactivity levels in the images. In the present study a more extensive and quantitative analysis of the whole-animal biodistribution of radioactive ethanol in rats was undertaken using phosphoimaging. Tissue dissection and counting experiments in mice were also conducted to determine the time-course and relative proportions of unchanged [1-

^{14}C]ethanol versus radiolabeled metabolites in various organs. Additionally, the effect of an alcohol dehydrogenase inhibitor on the radioactivity accumulation was evaluated. The goal of the [^{14}C]ethanol experiments in the present study was to identify sites of concentration of ethanol or its metabolites that may contribute to toxicological and pharmacokinetic characteristics of this substance.

Materials and Methods

Animals and drugs: Tissue dissection and counting studies were performed using male Swiss-Webster mice (Taconic farms, Germantown, NY) weighing between 20-30 g. Autoradiographic studies were performed using male Sprague-Dawley rats (Taconic, Germantown, NY) between 200 – 350 g. [1-^{14}C]ethanol (1 mCi/ml in ethanol) was obtained from American Radiolabeled Chemicals (St. Louis, MO). 4-methylpyrazole was obtained from Sigma-Aldrich (St. Louis, MO). All animal studies were approved by the Brookhaven National Laboratory animal care and use committee.

[1-^{14}C]ethanol biodistribution in mice. Mice were administered 1.6 mg (2 μCi; 72 KBq) [1-^{14}C]ethanol in saline via a tail vein and sacrificed by decapitation after 5 – 60 min. A blood sample was collected in a heparinized tube at the time of sacrifice and centrifuged to obtain plasma. Organs were dissected, frozen and weighed. Each organ was then homogenized in 2 ml of CAPS buffer, pH 10.0 and the homogenate divided into two portions. One portion was counted directly by liquid scintillation counting to determine total radioactivity in the tissue. The

second portion was used to determine the percentage of radioactivity in the tissue that was non-volatile. For this 0.5 ml unlabeled ethanol was added and the homogenate was evaporated to dryness overnight under vacuum. The dried homogenate was resolubilized in Solvable (Packard, Meriden, CT) and radioactivity counted in a liquid scintillation counter (Tricarb 1600, Packard). Alkaline conditions were used in the drying step to retain any radiolabeled acetate or bicarbonate as salts. Thus volatile radioactivity most likely represents unmetabolized [1-^{14}C]ethanol, although a small fraction could represent the proximal metabolite, [^{14}C]acetaldehyde. [1-^{14}C]ethanol spiked into one of the tissue samples was used to verify effective removal of volatile [1-^{14}C]ethanol by the drying step (approximately 94 %) in initial studies.

Whole-body autoradiography in rats: Rats were lightly anesthetized with isoflurane and a catheter secured in a tail vein. They were then allowed to awaken in a restraint device, administered 32 mg (40 μCi; 1.4 MBq) [1-^{14}C]ethanol in saline via the tail vein catheter and returned to their home cage. After either 15 min or 60 min following the [1-^{14}C]ethanol administration the rats were sacrificed by isoflurane overdose followed by snap freezing in a dry ice-hexane slurry. A blood sample was taken immediately prior to freezing the animal by cardiac puncture. For autoradiography, the frozen carcasses were sectioned using a whole-body cryosectioning instrument (custom-made) and the frozen sections covered in Mylar film and exposed to phosphor screens at –30^{O}C to prevent loss of [1-^{14}C]ethanol from the section. Exposure to the phosphor screens was continued for 40 h following which the screens were removed and scanned in a phosphorimager to image radioactivity. To enable quantification of the radioactivity levels in the sections, tissue punches were made in various locations in the sections (liver, rump and shoulder) using a 12 mm diameter cork borer, followed by weighing

and digestion of the tissue punches in Solvable® (Packard), addition of scintillation cocktail and counting in a scintillation counter.

To determine the radioactivity accounted for by non-volatile metabolites, sections from one rat at each sacrifice time point were subjected to a freeze-drying procedure and then reimaged on the phosphor screens.

Data analysis: For the mouse [1-^{14}C]ethanol biodistribution study, D.P.M. values were converted to % ID/g. To calculate the percentage of radioactivity that was non-volatile, the radioactivity following vacuum drying of the homogenates was divided by that in the original homogenates.

For the whole-body autoradiography in rats, mean pixel values for regions-of interest (ROIs) drawn over the images were converted to D.P.M. values by comparison with the direct scintillation counting of punches taken from the sections and the radioactive blood sample. Radioactive gelatin standards placed on each plate were additionally used to verify the D.P.M. values and the linearity of the phosphor screen response. D.P.M. values were then converted to % injected dose/g (% ID/g) by assuming an average tissue density of 1 g/ml and dividing by radioactive dose of ^{14}C administered to the animal.

For the whole body autoradiograph sections subjected to freeze-drying, quantitation was similar to that in the frozen sections except that D.P.M./g values in the tissue punches taken from the sections were converted to D.P.M./g original wet weight by recording the loss of weight in adjacent punches from the drying step. This was to facilitate direct comparison of radioactivity levels in the dehydrated versus frozen sections.

DMD Fast Forward. Published on June 19, 2008 as DOI: 10.1124/dmd.107.020271
This article has not been copyedited and formatted. The final version may differ from this version.

Results

[1-^{14}C]ethanol biodistribution in mice. A study on the time-course of [1-^{14}C]ethanol biodistribution following intravenous administration was conducted in mice (fig. 1). Following administration, radioactivity was present in all organs dissected. After 60 min, radioactivity levels declined from their initial values by between 60 to 75 %. The decline of tissue radioactivity in the brain and kidney was approximately in proportion to that in the plasma whereas that in the liver was slower. At all time points, the brain contained significantly less radioactivity than that in the other tissues.

To determine the percentage of tissue radioactivity at the different time points that was accounted for by volatile [1-^{14}C]ethanol relative to that of non-volatile [1-^{14}C]ethanol metabolites, a sample of the tissue homogenates from each mouse was vacuum dried under alkaline conditions prior to counting. This procedure indicated that the majority of the radioactivity in the tissues was accounted for by non-volatile [1-^{14}C] metabolites, even at the 5 min time point (fig. 1). Similar percentages of non-volatile radioactivity (89 – 99 % non-volatile at 60 min) were also observed in spleen, muscle, lungs and intestine (data not shown).

Whole-body autoradiography in rats. To obtain a more detailed image of the radioactivity distribution following [1-^{14}C]ethanol administration, a whole-body autoradiography study was conducted in rats (fig. 2 and table 1). Radioactivity following intravenous [1-^{14}C]ethanol administration in the rat showed a widespread distribution amongst body organs, especially at the early (15 min) time point. Highest levels were apparent in the Harderian glands, salivary and

preputial glands and in the pancreas. Significant levels were also present in the liver, lungs, stomach wall and bone marrow. Brain levels of radioactivity were below those in the blood at both the early and late (60 min) time points.

To estimate the relative proportions of radioactivity in the sections accounted for by volatile ethanol versus non-volatile radiolabeled ethanol metabolites, sections from one animal from each of the 15 and 60 min time points were freeze-dried and re-imaged (fig. 3 and table 2). When calculated relative to the original wet weight of the section, the overall radioactivity levels were lower in the dehydrated sections compared to that in the corresponding frozen sections, reflecting a loss of volatile [1-^{14}C]ethanol from the section. The greatest difference was apparent at the 15 min time point. At the 60 min time point only a minor level of the radioactivity was represented by volatile [1-^{14}C]ethanol in most tissues examined. However, some organ-to-organ differences in the amount of radioactivity accounted for by [1-^{14}C]ethanol were observed, with greatest levels of volatile radioactivity observed in the Harderian and especially the preputial glands and the lowest levels in the liver, kidney and pancreas.

To gain further insight into the relative contributions of [1-^{14}C]ethanol versus [^{14}C]ethanol metabolites in accounting for the distribution of radioactivity in various organs, two rats were administered the alcohol dehydrogenase inhibitor, 4-methylpyrazole (30 mg/kg, i.p.), 30 min prior to the [1-^{14}C]ethanol administration and sacrificed at 15 or 60 min following ^{14}C administration (fig. 4). After imaging of the sections, the sections were freeze-dried and re-imaged as previously. When compared to the untreated rats, in the 4-methypyrazle treated rats, the % ID/g values for ^{14}C (table 3) were significantly higher in the brain but lower in the pancreas and Harderian glands at both the 15 and 60 min time points. % ID/g values in the heart, kidney, liver, muscle and preputial glands though were approximately similar. Freeze-drying

and re-imaging the sections indicated that a much higher percentage of the radioactivity was volatile in the 4-methylpyrazole treated animals than in untreated animals, especially at the 60 min time point, this being consistent with inhibition of [1-^{14}C]ethanol metabolism by this compound.

Discussion

The main pathway for initial ethanol metabolism in animals is via alcohol dehydrogenase. This enzyme is most abundant in the liver, but lower levels are also found in other organs (Kovar et al., 1983). Following oxidization of ethanol to acetaldehyde, the acetaldehyde is oxidized further to acetate by aldehyde dehydrogenase. The acetate may then enter the tricarboxylate cycle (Isselbacher and Greenberger, 1964a; Isselbacher and Greenberger, 1964b) or the long-chain fatty acid synthesis pathway (Hakkinen and Kulonen, 1959; Smith and Newman, 1960). Carbon atoms from labeled acetate are ultimately oxidized to carbon dioxide by the tricarboxylate cycle, but are also incorporated into other compounds, including the amino acids glutamate and aspartate, that are metabolically connected to cycle intermediates. Thus depending on the time after [1-^{14}C]ethanol administration and the physiological state of the animal, residual radioactivity from [1-^{14}C]ethanol will represent different combinations of ethanol, acetaldehyde, acetate, bicarbonate, intermediary metabolites, and more complex molecules.

In the mouse experiment in the present study, overall radioactivity levels in the brain, liver and kidney declined in approximate proportion with that in the plasma. Interestingly, a majority of the radioactivity in the plasma and tissues was in the form of non-volatile

[^{14}C]metabolites, even at the 5 min time point. Ethanol is metabolized under saturating conditions at a constant rate (zero order) of about 700 mg/kg/h in the mouse (Marshall and Owens, 1955) and the actual amount of ethanol delivered to the mice in the current study was relatively small (80 mg/Kg). This may account for the relatively rapid conversion of [1-^{14}C]ethanol to non-volatile metabolite observed in the study.

A more detailed picture of the biodistribution of radiolabeled ethanol and its metabolites amongst various organs was obtained in the present study using whole-body autoradiography in rats. This revealed high concentration of radioactive material at both the 15 min and 60 min time points in glandular structures such as the Harderian, salivary and preputial glands as well as in the liver and pancreas. In the case of the liver, the high levels of radioactivity in this organ is consistent with its central role in ethanol metabolism and in biosynthesis of proteins and complex lipids.

Examination of the loss in radioactivity from freeze-drying the sections indicated that, at the 15 min time point, approximately half of the radioactivity in the sections was volatile, assumed to mostly represent that due to unmetabolized [1-^{14}C]ethanol. However, at the 60 min time point only a minor loss in radioactivity by drying the sections was observed. The latter indicates that most of the ethanol had been converted to non-volatile metabolites by this time point. The time-course for conversion of ethanol to non-volatile metabolites was slower in the rat autoradiographic studies than in the mouse studies, consistent with the larger body size of this species. By way of comparison, blood half-life of ethanol following a pharmacological intravenous dose (250 mg/kg) in rats is approximately 30 min (Caballeria et al., 1989). This is slower than the rate of loss of volatile material observed in the present rat autoradiographic

study, although since lower ethanol doses were used in the present study (~ 90 mg/kg) a faster rate of metabolism in the present study is to be expected.

Especially notable in the current study was the high concentration of radioactivity in the pancreas, which was significantly above that in most of the other major organs, including the liver. High levels of radioactivity in the pancreas were also apparent in whole-body autoradiographic images of a monkey fetus taken following [^{14}C]ethanol administration to the mother in the study by Ho et al. (1972). These observations are intriguing in view of the well-documented occurrence of pancreatitis in chronic alcoholism (Singh and Simsek, 1990; Apte et al., 1998; Apte et al., 2006). It is thus tempting to speculate that the susceptibility of this organ to damage may be related to a high propensity to accumulate ethanol and/or reactive metabolites from ethanol metabolism. Pancreatic acinar cells are capable of metabolizing ethanol via both the oxidative and non-oxidative pathways (Haber et al., 1998; Haber et al., 2004; Gukovskaya et al., 2002). The latter occurs by esterification of ethanol with fatty acids, resulting in the formation of fatty acid ethyl esters (Wilson and Apte, 2003). The products of both oxidative metabolism of ethanol (acetaldehyde and reactive oxygen species) and non-oxidative metabolism of ethanol (fatty acid ethyl esters) have deleterious effects on pancreatic tissue (Nordback et al., 1991; Wilson and Apte, 2003). In the present study the accumulation of radioactivity from [^{14}C]ethanol in the pancreas was diminished in the rats given prior treatment with 4-methylpyrazole. This suggest that at least part of the accumulation and trapping of ^{14}C in this organ involves metabolism of [^{14}C]ethanol by alcohol dehydrogenase rather than via non-oxidative pathways. The metabolism and trapping of radiolabeled ethanol may occur either directly by the organ itself or by the accumulation and trapping of circulating ^{14}C metabolites (e.g. acetate). Further studies with radiolabeled ethanol and ethanol metabolites on isolated

pancreatic tissue would be needed distinguish between these possibilities. In comparing the relative importance of the oxidative and non-oxidative pathways in the pancreas, it has been observed that in isolated rat pancreatic acini incubated in alcohol, the rate of oxidative metabolism is 20 fold higher than the rate of non-oxidative metabolism (Gukovskaya et al., 2002; Haber et al., 2004). This would be consistent with the accumulation of ^{14}C in the pancreas observed in the present study resulting primarily from oxidative pathways of metabolism. However, it should also be noted that fatty acid ethyl ester formation is much enhanced in animals treated with 4-methylpyrazole (Manautou and Carlson, 1991), suggesting that these compounds may nonetheless have made up a significant component of the residual non-volatile metabolites in the case of the 4-methylpyrazole treated animals.

The preputial gland was observed to exhibit a high uptake of radiolabel in the current study, with most of the radioactivity volatile, even at the 60 min time point. The preputial gland of rodents appears to be specialized for synthesis of pheromones (Novotny, 2003), but the human preputial gland has been implicated as a target of maternal drinking (Amankwah et al., 1982). Since ethanol is not expected to be a substrate for active transport processes, ethanol accumulation in this structure could be explained by passive transfer of ethanol from blood during the initial distribution phase to a tissue compartment from which it is denied ready access back to the circulation. Because of the involvement of the preputial gland in pheromone synthesis, it is possible that the trapping mechanism may involve incorporation of the radiolabel into a volatile pheromone compound. Since the accumulation of [^{14}C]ethanol in the preputial gland was little affected by prior dosing of the animal with 4-methylpyrazole this may suggest that any such metabolic trapping mechanism for ethanol in this gland occurs mostly via a non-

oxidative mechanism, such as esterification for example, rather than via products from alcohol dehydrogenase activity.

Particularly high levels of radiolabel were observed in the present autoradiographic study in the Harderian gland. The Harderian glands are exocrine glands that are present in rodents, birds, amphibians and reptiles but are vestigial in primates (Buzzell, 1996). Their main secretory product is lipid (Buzzell, 1996). The marked accumulation of radiolabel from ethanol in these organs is thus intriguing. The trapping mechanism appears to involve at least in part alcohol dehydrogenase activity, since the accumulation of radiolabel in these organs was significantly lowered in the rats given prior treatment with 4-methylpyrazole.

The level of radioactivity in the brain following [^{14}C]ethanol administration to the rats was low and below that in the blood. This suggests an exclusion of charged or polar circulating radiolabeled metabolites of ethanol by the blood-brain barrier. This is supported by the fact that a higher level of radiolabel was observed in the brain when the rats were pretreated with 4-methylpyrazole, in which plasma levels of unmetabolized [^{14}C]ethanol will be higher. An obvious candidate for the [^{14}C] metabolites which were present in the brain in the untreated rats is [^{14}C]acetate, since recent work implicates acetate as an energy substrate of the brain, especially during alcohol intoxication (Cruz et al., 2005; Volkow et al., 2006).

Although radioactivity in the blood and most organs dropped between the 15 min and 60 min sacrifice time points in the rats, radioactivity levels increased substantially in the lumen of the small intestine, likely reflecting partial elimination of ethanol or its metabolites via the hepatobiliary system.

In conclusion, our quantitative whole-body imaging study of intravenous [1-^{14}C]ethanol using phosphor-screen autoradiography supplements older non-quantitative studies using

photographic film. Highest concentrations of ^{14}C were imaged in Harderian and preputial glands, intestinal contents, and pancreas. This study is the first autoradiographic study to image the whole-body biodistribution of radiolabeled ethanol in a quantitative manner, and significantly extends earlier and less detailed non-quantitative studies. The study also provides initial animal data to support future PET studies to examine the biodistribution and pharmacokinetics [^{11}C] radiolabeled ethanol in clinical studies.

References

Akesson C (1974) Autoradiographic studies on the distribution of ^{14}C-2-ethanol and its nonvolatile metabolites in the pregnant mouse. *Arch Int Pharmacodyn Ther* **209:**296-304.

Amankwah KS, Weberg AD and Kaufmann RC (1982) Ultrastructural changes in preputial neural tissues: Effects of maternal drinking. *Early Hum Dev* **6:**375-380.

Apte MV, Haber PS, Norton ID and Wilson JS (1998) Alcohol and the pancreas. *Addiction Biology* **3:**137-150.

Apte MV, Pirola RC and Wilson JS (2006) Battle-scarred pancreas: role of alcohol and pancreatic stellate cells in pancreatic fibrosis. *J Gastroenterol Hepatol* **21 Suppl 3:**S97-S101.

Buzzel GR (1996) The Harderian gland: Perspectives. *Microsc. Res. Tech*. **34**: 2-5

Caballeria J, Baraona E, Rodamilans M and Lieber CS (1989) Effects of cimetidine on gastric alcohol dehydrogenase activity and blood ethanol levels. *Gastroenterology* **96:**388-392.

Cruz NF, Lasater A, Zielke HR and Dienel GA (2005) Activation of astrocytes in brain of conscious rats during acoustic stimulation: acetate utilization in working brain. *J Neurochem* **92:**934-947.

Gukovskaya AS, Mouria M, Gukovsky I, Reyes CN, Kasho VN, Faller LD and Pandol SJ (2002) Ethanol metabolism and transcription factor activation in pancreatic acinar cells in rats. *Gastroenterology* **122:**106-118.

Gulyas B, Vas A, Halldin C, Sovago J, Sandell J, Olsson H, Fredriksson A, Stone-Elander S and Farde L (2002) Cerebral uptake of [ethyl-^{11}C]vinpocetine and 1-[^{11}C]ethanol in cynomolgous monkeys: a comparative preclinical PET study. *Nucl Med Biol* **29:**753-759.

Hakkinen HM and Kulonen E (1959) Metabolic products from labelled ethanol. III. Chemical fractionation. *Arch Int Pharmacodyn Ther* **123:**21-33.

Haber PS, Apte MV, Applegate TL, Norton ID, Korsten MA, Pirola RC and Wilson JS (1998) Metabolism of ethanol by rat pancreatic acinar cells. *Journal of Laboratory and Clinical Medicine* **132:**294-302.

Haber PS, Apte MV, Moran C, Applegate TL, Pirola RC, Korsten MA, McCaughan GW and Wilson JS (2004) Non-oxidative metabolism of ethanol by rat pancreatic acini. *Pancreatology* **4:**82-89.

Ho BT, Idanpaan JE, Fritchie GE and McIsaac WM (1972) Placental transfer and tissue distribution of ethanol-1-^{14}C – An autoradiographic Study in Monkeys and Hamsters. *Quarterly Journal of Studies on Alcohol* **33:**485-492.

Isselbacher KJ and Greenberger NJ (1964a) Metabolic effects of alcohol in the liver. *N Engl J Med* **270:**351-356.

Isselbacher KJ and Greenberger NJ (1964b) Metabolic effects of alcohol on the liver. *N Engl J Med* **270:**403-410.

Jamal M, Ameno K, Kumihashi M, Ameno S, Kubota T, Wang WH and Ijiri I (2003) Microdialysis for the determination of acetaldehyde and ethanol concentrations in the striatum of freely moving rats. *J Chromatogr B Analyt Technol Biomed Life Sci* **798:**155-158.

Kovar J, Racek P and Vlckova V (1983) Alcohol-dehydrogenase activity and isoenzyme distribution in the organs of cow, pig and sheep. *Comp Biochem Physiol B* **76:**161-165.

Manautou JE and Carlson GP (1991) Ethanol-induced fatty acid ethyl ester formation in vivo and in vitro in rat lung. *Toxicology* **70:**303-312.

Marshall EK, Jr. and Owens AH, Jr. (1955) Rate of metabolism of ethyl alcohol in the mouse. *Proc Soc Exp Biol Med* **89:**573-576.

Nordback IH, Macgowan S, Potter JJ and Cameron JL (1991) The Role of Acetaldehyde in the Pathogenesis of Acute Alcoholic Pancreatitis. *Annals of Surgery* **214:**671-678.

Novotny MV (2003) Pheromones, binding proteins and receptor responses in rodents. *Biochem Soc Trans* **31:**117-122.

Peris J, Zharikova A, Li Z, Lingis M, MacNeill M, Wu MT and Rowland NE (2006) Brain ethanol levels in rats after voluntary ethanol consumption using a sweetened gelatin vehicle. *Pharmacol Biochem Behav* **85:**562-568.

Quertemont E, Green HL and Grant KA (2003) Brain ethanol concentrations and ethanol discrimination in rats: effects of dose and time. *Psychopharmacology* **168:**262-270.

Richardson WR, Schaefer GJ, Bonsall RW and Michael RP (1987) Effects of ethanol on motor-activity and its relation to blood, brain and tissue concentrations. *Federation Proceedings* **46:**546-546.

Robinson DL, Lara JA, Brunner LJ and Gonzales RA (2000) Quantification of ethanol concentrations in the extracellular fluid of the rat brain: In vivo calibration of microdialysis probes. *J Neurochem* **75:**1685-1693.

Singh M and Simsek H (1990) Ethanol and the pancreas. Current status. *Gastroenterology* **98:**1051-1062.

Smith ME and Newman HW (1960) Ethanol-1-^{14}C and acetate-1-^{14}C incorporation into lipid fractions in the mouse. *Proc Soc Exp Biol Med* **104:**282-284.

Smolen TN and Smolen A (1989) Blood and brain ethanol concentrations during absorption and distribution in long-sleep and short-sleep mice. *Alcohol* **6:**33-38.

Sunahara GI, Kalant H, Schofield M and Grupp L (1978) Regional distribution of ethanol in the rat brain. *Can J Physiol Pharmacol* **56:**988-992.

Volkow ND, Wang GJ, Franceschi D, Fowler JS, Thanos PK, Maynard L, Gatley SJ, Wong C, Veech RL, Kunos G and Li TK (2006) Low doses of alcohol substantially decrease glucose metabolism in the human brain. *Neuroimage* **29:**295-301.

Wilson JS and Apte MV (2003) Role of alcohol metabolism in alcoholic pancreatitis. *Pancreas* **27:**311-315.

Footnotes

Financial support: This work was funded by NIH grant No. 5R21AA014018 and performed under Brookhaven Science Associates contract No. DE-AC02-98CH1-886 with the U.S. Department of Energy.

Reprint requests: Dr. A.N. Gifford, Medical Department, Brookhaven National Laboratory, Upton NY 11973.

Tel: 631-344-7069; Fax: 631-344-5311; email: gifforda@bnl.gov

* Current affiliation: Department of Pharmaceutical Sciences, School of Pharmacy, Northeastern University, Boston, MA 02115

Figure Legends

Fig. 1. Time course of total radioactivity (filled squares) and the percentage of tissue radioactivity in the form of non-volatile metabolites (open circles) following intravenous administration of [1-^{14}C]ethanol to mice.

Fig. 2. Whole body autoradiography in a rat sacrificed at 15 min (sections A and B) and 60 min (sections C and D) following intravenous administration of [1-^{14}C]ethanol.

Fig. 3. Comparison of the radioactivity in whole-body autoradiography sections before and after freeze-drying sections to evaporate volatile radioactivity. Sections were taken from an animal sacrificed at 15 min (section A and B) or 60 min (section C and D) after [1-^{14}C]ethanol administration. Images on the left are before drying the sections and on the right after drying the sections.

Fig. 4. Whole body autoradiography in rats pretreated with 4-methypyrazole prior to [1-^{14}C]ethanol administration. Animals were sacrificed at 15 min (section A) or 60 min (section B) following [1-^{14}C]ethanol.

DMD Fast Forward. Published on June 19, 2008 as DOI: 10.1124/dmd.107.020271
This article has not been copyedited and formatted. The final version may differ from this version.

TABLE 1

Regions-of-interest (ROI) analysis to quantify levels of radioactivity in various tissues from whole-body autoradiography in rats.

Data represent the means (± SEM) from whole-body autoradiography conducted on three separate rats at each of the 15 min and 60 min sacrifice time points. Values are expressed as % ID/g in the left column and as tissue to blood ratios in the right column.

	15 min		60 min	
Organ	**%ID/g**	**Tissue:Blood ratio**	**%ID/g**	**Tissue:Blood ratio**
Adrenal gland	0.28 ± 0.03	0.90 ± 0.03	0.25 ± 0.05	1.68 ± 0.12
Blood	0.31 ± 0.02	1.00 ± 0.00	0.15 ± 0.02	1.00 ± 0.00
Bone Marrow	0.35 ± 0.01	1.13 ± 0.07	0.38 ± 0.05	2.56 ± 0.07
Brain	0.16 ± 0.03	0.49 ± 0.05	0.13 ± 0.02	0.87 ± 0.03
Cecum	0.14 ± 0.02	0.43 ± 0.05	0.27 ± 0.05	1.79 ± 0.04
Epididymis	0.22 ± 0.03	0.70 ± 0.13	0.20 ± 0.03	1.33 ± 0.09
Eye	0.20 ± 0.04	0.64 ± 0.10	0.18 ± 0.02	1.26 ± 0.82
Fat (neck)	0.31 ± 0.04	0.99 ± 0.11	0.34 ± 0.10	2.31 ± 0.70
Harderian gland	1.42 ± 0.15	4.55 ± 0.21	3.00 ± 0.95	19.32 ± 3.11
Heart	0.39 ± 0.03	1.27 ± 0.09	0.19 ± 0.03	1.25 ± 0.03
Intestine contents	0.60 ± 0.24	1.89 ± 0.78	1.49 ± 0.47	10.01 ± 2.93
Intestine wall	0.45 ± 0.06	1.43 ± 0.10	0.54 ± 0.13	3.52 ± 0.23
Kidney cortex	0.86 ± 0.14	2.74 ± 0.25	0.44 ± 0.07	2.93 ± 0.07
Kidney medulla	0.39 ± 0.08	1.25 ± 0.17	0.26 ± 0.04	1.77 ± 0.17
Liver	0.44 ± 0.07	1.39 ± 0.13	0.45 ± 0.07	3.05 ± 0.25
Lung	0.43 ± 0.05	1.38 ± 0.09	0.36 ± 0.05	2.40 ± 0.15
Muscle	0.26 ± 0.03	0.81 ± 0.05	0.14 ± 0.02	0.93 ± 0.07
Pancreas	0.75 ± 0.09	2.39 ± 0.19	0.89 ± 0.15	5.94 ± 0.05
Preputial gland	1.00 ± 0.01	3.44 ± 0.34	1.18 ± 0.16	7.93 ± 0.41
Prostrate gland	0.37 ± 0.05	1.25 ± 0.06	0.36 ± 0.05	2.56 ± 0.59
Salivary gland	0.59 ± 0.04	1.88 ± 0.06	0.71 ± 0.14	4.71 ± 0.35
Seminal vesicle	0.17 ± 0.01	0.55 ± 0.02	0.10 ± 0.08	0.61 ± 0.17
Spinal cord	0.13 ± 0.01	0.42 ± 0.02	0.13 ± 0.03	0.85 ± 0.06
Spleen	0.55 ± 0.06	1.76 ± 0.15	0.45 ± 0.29	2.83 ± 0.36
Stomach contents	0.08 ± 0.02	0.25 ± 0.05	0.08 ± 0.04	0.49 ± 0.17
Stomach wall	0.50 ± 0.05	1.61 ± 0.13	0.54 ± 0.07	3.67 ± 0.15
Testis	0.21 ± 0.02	0.68 ± 0.09	0.24 ± 0.06	1.58 ± 0.14
Thymus	0.33 ± 0.00	1.07 ± 0.06	0.30 ± 0.04	2.03 ± 0.06

DMD Fast Forward. Published on June 19, 2008 as DOI: 10.1124/dmd.107.020271
This article has not been copyedited and formatted. The final version may differ from this version.

TABLE 2

Region-of-interest (ROI) analysis to quantify loss of radioactivity in the whole-body sections from freeze-drying the sections.

% ID/g values calculated from the ROIs drawn prior to drying the sections are shown on the left and the approximate percent radioactivity remaining in the ROIs following drying on the right. Data from one animal for each of the two time points.

	15 min		**60 min**	
Organ	**%ID/g**	**% Remaining after dehydration**	**%ID/g**	**% Remaining after dehydration**
Blood	0.31	21 %	0.11	87 %
Brain	0.15	39 %	0.09	87 %
Harderian gland	1.47	32 %	2.24	65 %
Heart	0.34	55 %	0.14	93 %
Kidney	0.54	53 %	0.29	100 %
Liver	0.39	42 %	0.33	99 %
Muscle	0.23	43 %	0.10	87 %
Pancreas	0.61	61 %	0.68	89 %
Preputial gland	1.00	7 %	1.01	19 %

TABLE 3

Quantification of the levels of radioactivity in various tissues from whole-body autoradiography in two rats pretreated with 4-methylpyrazole.

% ID/g values calculated from the ROIs drawn in the sections prior to freeze-drying are shown on the left and the approximate percent radioactivity remaining in the ROIs following drying and re-imaging the sections on the right. Data are from one animal for each time point.

	15 min		60 min	
Organ	**%ID/g**	**% Remaining after dehydration**	**%ID/g**	**% Remaining after dehydration**
Blood	0.34	11 %	0.26	17 %
Brain	0.27	14 %	0.17	28 %
Harderian gland	0.53	28 %	0.71	45 %
Heart	0.29	12 %	0.22	17 %
Kidney	0.45	36 %	0.37	48 %
Liver	0.36	19 %	0.34	26 %
Muscle	0.27	11 %	0.22	14 %
Pancreas	0.42	24 %	0.44	41 %
Preputial gland	0.82	26 %	1.18	13 %

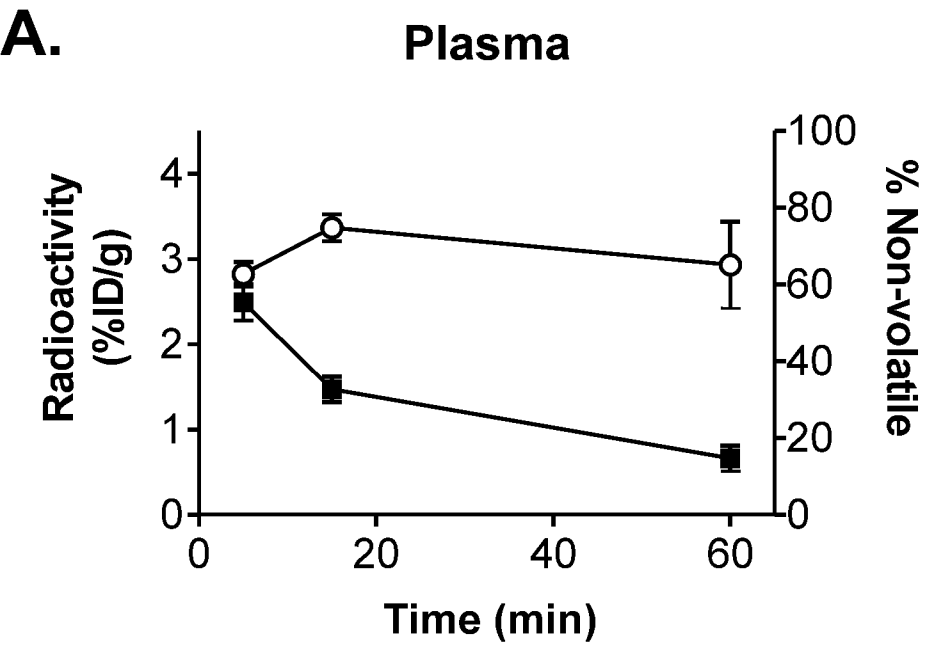

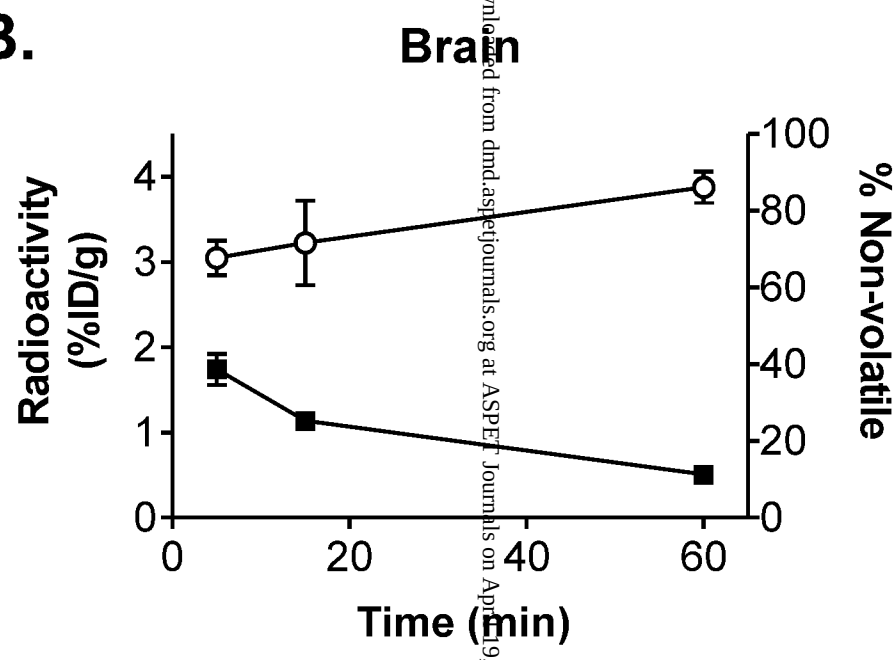

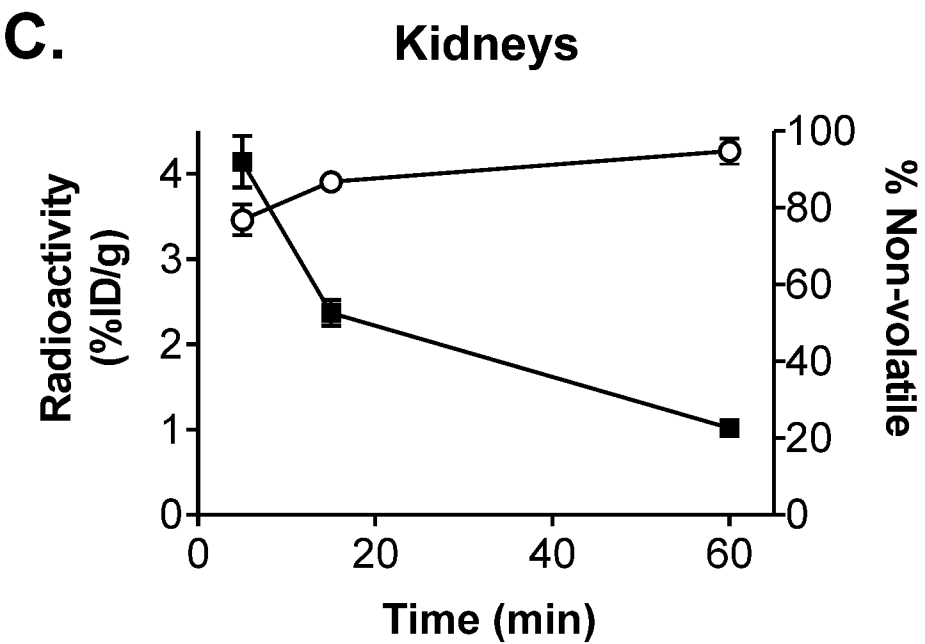

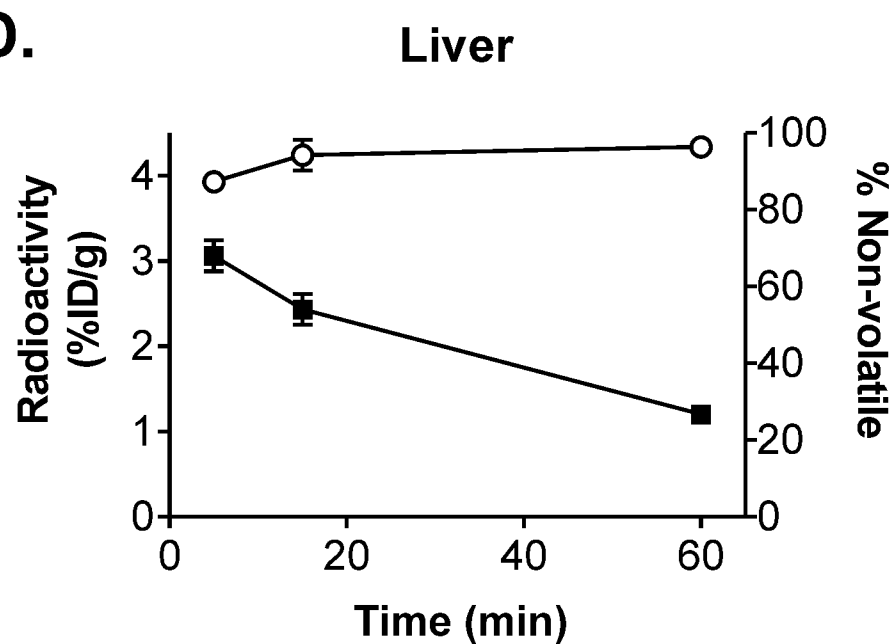

DMD Fast Forward. Published on June 19, 2008 as DOI: 10.1124/dmd.107.020271
This article has not been copyedited and formatted. The final version may differ from this version.

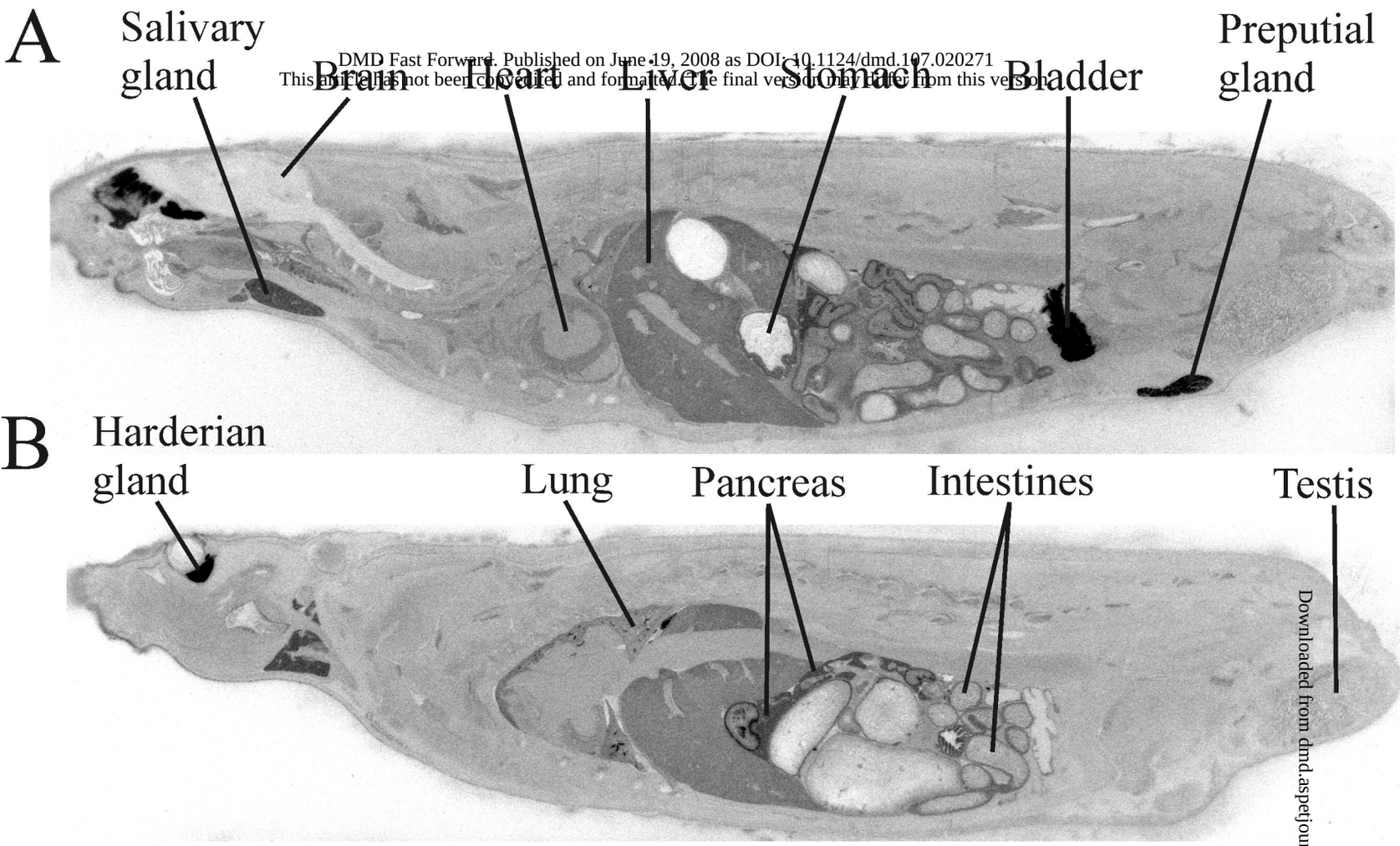

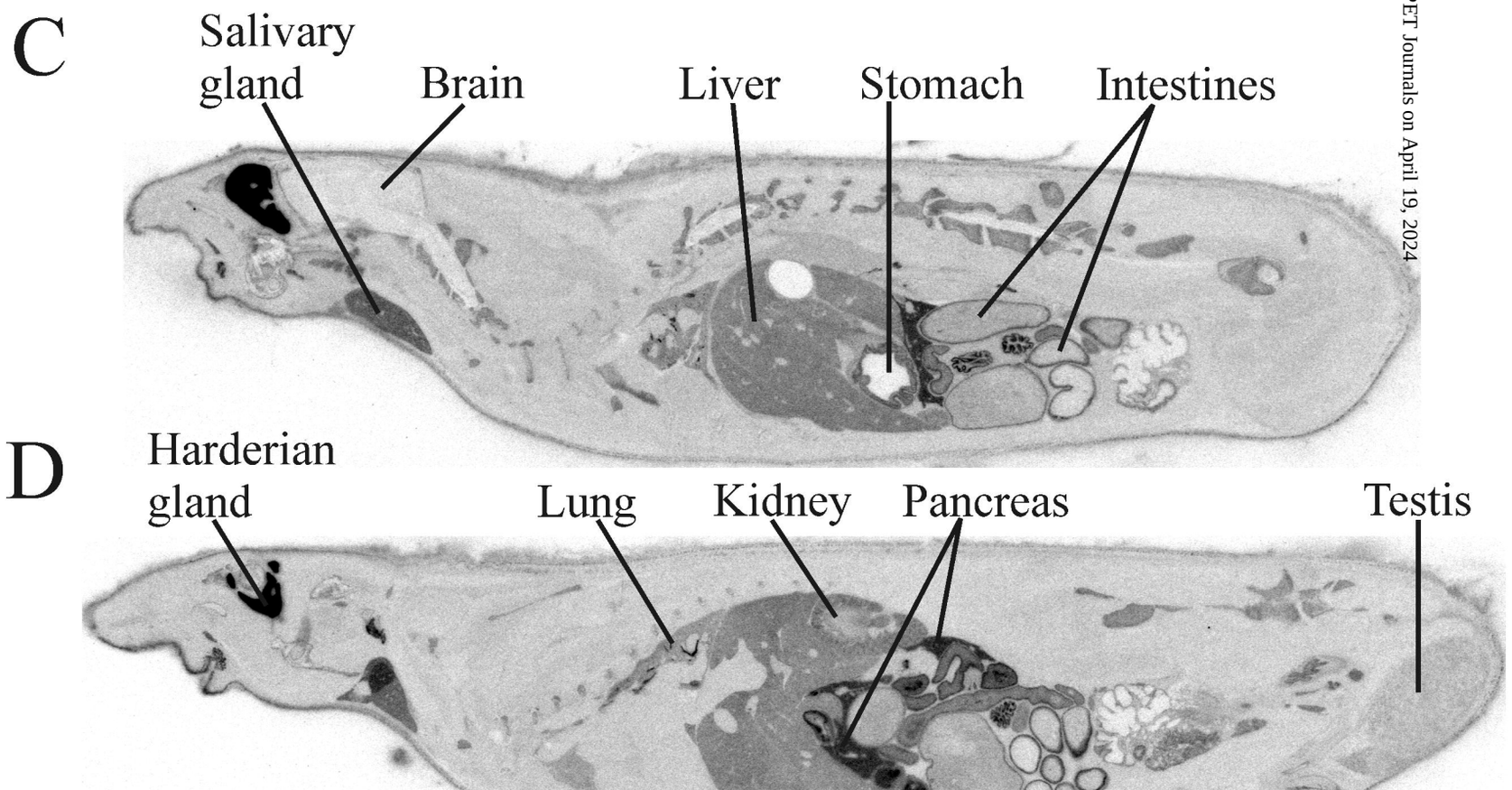

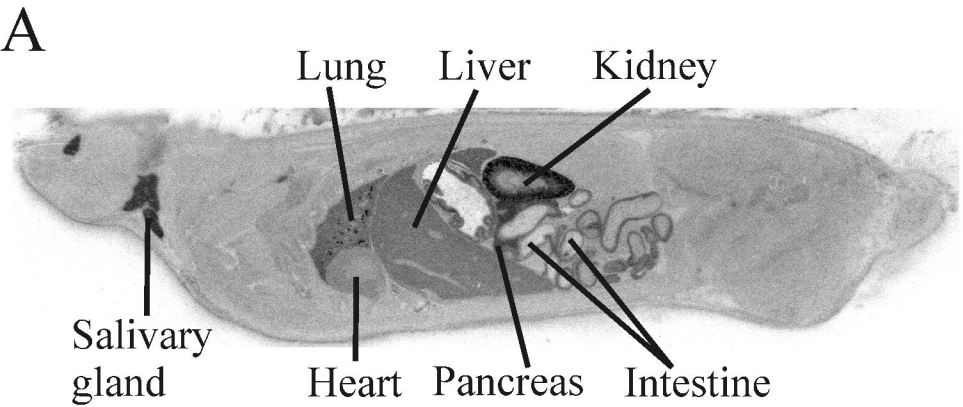

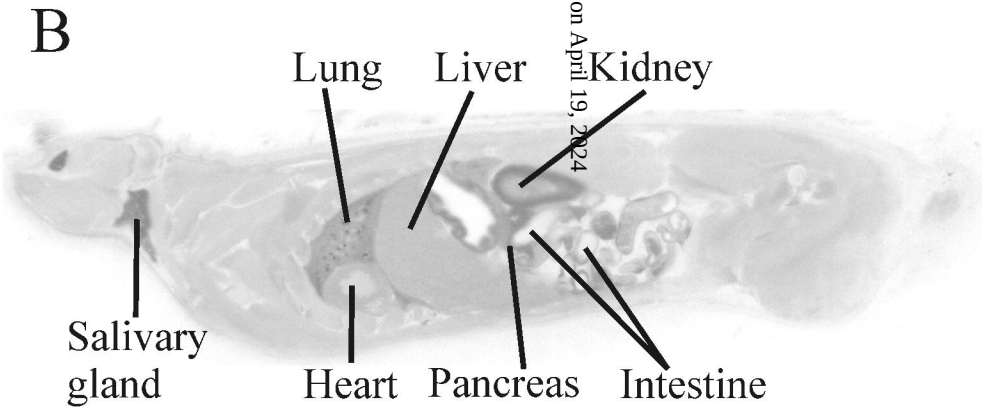

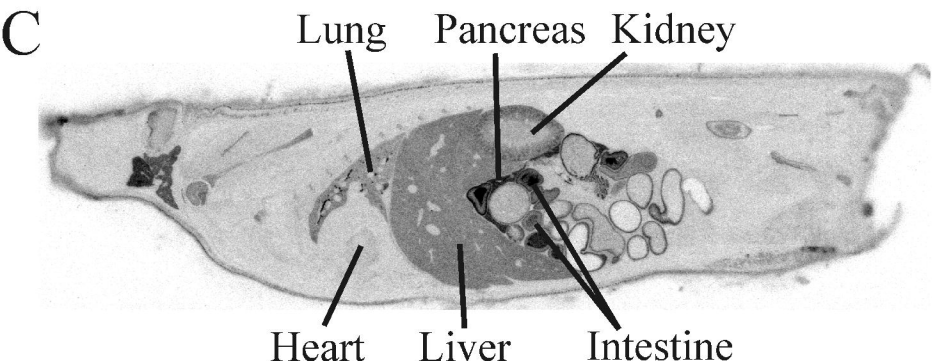

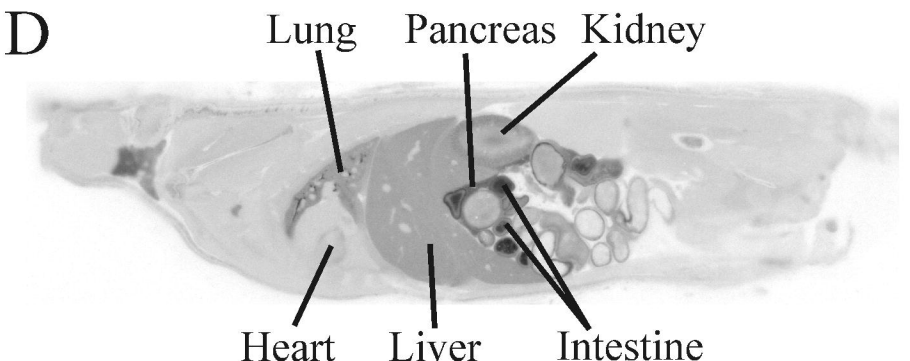

Figure 4